

DOCUMENT CONTROL DATA - R & D

(Security classification of title, body of abstract and indexing annotation must be entered when the overall report is classified)

1. ORIGINATING ACTIVITY (Corporate author) Naval Research Laboratory Washington, D.C. 20390		2a. REPORT SECURITY CLASSIFICATION Unclassified	
		2b. GROUP	
3. REPORT TITLE CORROSION FATIGUE CRACK GROWTH BEHAVIOR ABOVE AND BELOW K_{Isc}			
4. DESCRIPTIVE NOTES (Type of report and inclusive dates) A final report on one phase of a continuing problem.			
5. AUTHOR(S) (First name, middle initial, last name) J.P. Gallagher			
6. REPORT DATE May 28, 1970		7a. TOTAL NO. OF PAGES 22	7b. NO. OF REFS 24
8a. CONTRACT OR GRANT NO. NRL Problem M01-08		9a. ORIGINATOR'S REPORT NUMBER(S) NRL Report 7064	
b. PROJECT NO. RR 007-01-46-5416		9b. OTHER REPORT NO(S) (Any other numbers that may be assigned this report)	
c.			
d.			
10. DISTRIBUTION STATEMENT This document has been approved for public release and sale; its distribution is unlimited.			
11. SUPPLEMENTARY NOTES		12. SPONSORING MILITARY ACTIVITY Department of the Navy (Office of Naval Research), Washington, D.C. 20360	
13. ABSTRACT This report describes how the frequency of the applied load can be used to separate the influences of environmental attack and fatigue loading in corrosion fatigue crack propagation studies. Two types of corrosion fatigue cracking behavior were experienced; these are designated with respect to material susceptibility to stress-corrosion cracking, i.e., behavior above and below the environmental threshold stress intensity K_{Isc} . A material with known susceptibility to sustained-load cracking, 4340 steel, was chosen for the above K_{Isc} study, while HY-80 steel, a material with high resistance to corrosion attack, was selected for the below K_{Isc} investigation. The enhanced environmental fatigue cracking observed in HY-80 for stress intensity levels below K_{Isc} appears to require the new surface area generated by the fatigue loading, since the crack growth rates are predominately cycle-dependent. The corrosion fatigue crack growth in 4340 steel for stress intensity levels above K_{Isc} for all loading frequencies below 1 Hz were shown to be independent of the numbers of cycle, and cracking rates were noted to be completely controlled by the rate of environmental attack. The effect of applying cathodic protection potentials to both materials was to increase the cracking rates above those under freely corroding conditions, indicating that the environmental mechanism of attack was hydrogen embrittlement.			

14. KEY WORDS	LINK A		LINK B		LINK C	
	ROLE	WT	ROLE	WT	ROLE	WT
Fracture mechanics Corrosion fatigue behavior in steels Stress-corrosion cracking in steels Hydrogen cracking of steels						

CONTENTS

Abstract	ii
Problem Status	ii
Authorization	ii
INTRODUCTION	1
MATERIALS AND PROCEDURES	2
Material	2
Specimens	2
Load Control and Crack Measurement	4
Environments	4
RESULTS AND DISCUSSION	5
Fatigue in Vacuum	5
Corrosion Fatigue Crack Growth Rates Below K_{Isc}	6
Corrosion Fatigue Crack Growth Rates Above K_{Isc}	13
CONCLUSIONS	15
ACKNOWLEDGMENT	16
REFERENCES	17

ABSTRACT

This report describes how the frequency of the applied load can be used to separate the influences of environmental attack and fatigue loading in corrosion fatigue crack propagation studies. Two types of corrosion fatigue cracking behavior were experienced; these are designated with respect to material susceptibility to stress-corrosion cracking, i.e., behavior *above* and *below* the environmental threshold stress intensity $K_{I_{sc}}$. A material with known susceptibility to sustained-load cracking, 4340 steel, was chosen for the above $K_{I_{sc}}$ study, while HY-80 steel, a material with high resistance to corrosion attack, was selected for the below $K_{I_{sc}}$ investigation.

The enhanced environmental fatigue cracking observed in HY-80 for stress intensity levels below $K_{I_{sc}}$ appears to require the new surface area generated by the fatigue loading, since the crack growth rates are predominately cycle-dependent. The corrosion fatigue crack growth in 4340 steel for stress intensity levels above $K_{I_{sc}}$ for all loading frequencies below 1 Hz were shown to be independent of the numbers of cycles, and cracking rates were noted to be completely controlled by the rate of environmental attack. The effect of applying cathodic protection potentials to both materials was to increase the cracking rates above those under freely corroding conditions, indicating that the environmental mechanism of attack was hydrogen embrittlement.

PROBLEM STATUS

This report concludes one phase of the task; other work on the task is continuing.

AUTHORIZATION

NRL Problem M01-08
Task RR 007-01-46-5416

Manuscript submitted January 28, 1970.

CORROSION FATIGUE CRACK GROWTH BEHAVIOR ABOVE AND BELOW K_{Isc}

INTRODUCTION

The structural capability of engineering components subjected to cyclic loading while exposed to an environment can be completely destroyed by the joint action of two material attack mechanisms. This joint action, defined as corrosion fatigue, combines the effects of environmental and fatigue attack. Corrosion fatigue action has been noted to produce material damage for almost any combination of applied stress level, material, heat treatment, and corrosive agent (1), whereas the individual mechanisms promote attack only for unfortunate combinations of these parameters.

Only a limited number of investigators have performed systematic experimental studies to quantitatively determine the mechanical, metallurgical, and chemical parameters associated with the corrosion fatigue problem. Most investigators chose to isolate the individual mechanisms and study the parameters which excite these mechanisms to cause failure. These investigations have resulted in an understanding of how the fatigue and environmental attack mechanisms operate to cause the material damage leading to fracture:

1. The microscopic material damage produced by repeatedly applying loads to a component depends on the number of times that the loads are applied; i.e., fatigue damage is cycle dependent (i.e., dependent on the number of cycles).
2. Environmental damage is time dependent, because the environmental attack resulting from the contact of the environment with the material surface is strongly influenced by the time of exposure.

The fundamental difference in the character of the individual attack mechanisms reflects itself in the character of the corrosion fatigue attack.

The distinguishing characteristic of the corrosion fatigue attack is the ability of the combined fatigue and environmental action to nucleate and propagate cracks. This combined action usually results in component lives that are shorter than would be expected if only one of the attack mechanisms were operating. From fatigue studies conducted in nonaggressive environments, the character of the localized fatigue damage is noted to remain essentially constant throughout the life of the component. One special feature of the environmental attack is that the type of attack can change when loads are applied to the component or when components containing preexisting flaws are introduced into service. Under certain conditions, the attack can become a single localized action such as that observed in stress-corrosion cracking. Techniques have been used successfully to describe the propagation of stress-corrosion cracks (2) and to develop a fracture mechanics parameter K_{Isc} which provides the lower limit on the measurable crack growth regime (3).

The purpose of this investigation was to contrast the salt water corrosion fatigue crack propagation behaviors observed in the two regimes of no measurable sustained load crack propagation (below K_{Isc} behavior) and of measurable stress-corrosion cracking rates (above K_{Isc} behavior). A typical structural steel, HY-80 steel, having intermediate strength and high toughness, was selected for its high resistance to environmental

cracking under sustained load ($K_{I_{sc}} > 200 \text{ ksi } \sqrt{\text{in.}}$). A high-strength 4340 steel which was previously shown to be highly susceptible to environmental cracking under sustained loads was chosen for the above- $K_{I_{sc}}$ behavior study (4,5).

To determine the general character of the crack growth behaviors, the frequency of cyclic loading and the environmental condition were varied. Whenever one wishes to determine if an environment markedly decreases a material's resistance to fatigue damage, the first mechanical variable that should be considered is frequency of loading. This approach follows directly from the hypothesis: *If the environmental damage is time dependent and if the fatigue damage is cycle dependent, then variation of frequency allows the time-dependent action to occur while it holds the cycle-dependent action constant.* The results of both studies were compared to base line (vacuum) fatigue crack propagation data.

MATERIALS AND PROCEDURES

Material

The chemical compositions of the HY-80 and 4340 steels are given in Table 1. The HY-80 steel was tested in the mill-annealed condition, which would result in a minimum specified yield strength of 80 ksi. The 4340 steel was quenched and tempered to a 220-ksi 0.2% offset yield strength level according to the heat treatment schedule given here.

1. Austenitize 1600°F for 1 hour in salt bath
2. Oil quench
3. Temper 1 hour at 600°F in air
4. Water cool
5. Repeat steps 3 and 4
6. Surface grind, remove 0.020 in. from both sides of a specimen.

Rockwell measurements made on the finished specimens indicated a hardness of $49 \pm 1 R_c$.

Table 1
Chemical Compositions of Materials

Steel	C	Mn	P	Si	Ni	Cr	Mo	S	V	Cu	Al	Fe
4340	0.40	0.72	0.012	0.28	1.70	0.80	0.24					Remainder
HY-80	0.15	0.37	0.017	0.26	2.21	1.12	0.29	0.017	0.05	0.04	0.01	Remainder

Specimens

Two single-edge-notched specimens used in the study are shown in Fig. 1. Ten SEN 1 specimens were used in the HY-80 investigation, and eight SEN 2 specimens were used in the 4340 steel investigation. Stress intensity factors were determined using compliance data processed by a movable-strip technique (6). The stress intensity results are given in Figs. 2 and 3.

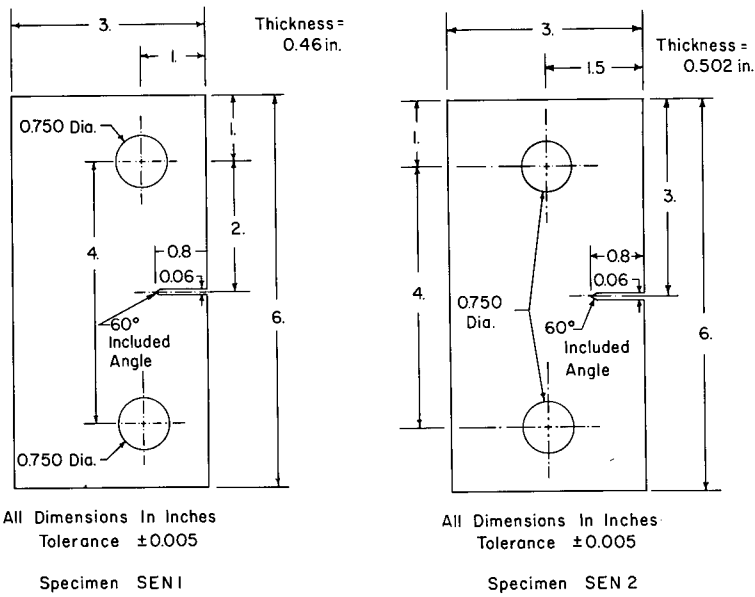


Fig. 1 - Specimen geometries for the single-edge-notched specimens SEN 1 and SEN 2

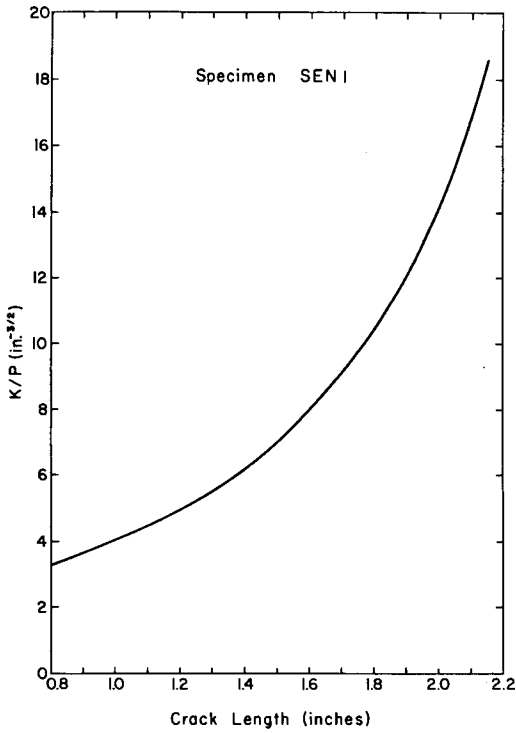


Fig. 2 - Stress intensity relationship between applied load and crack length for specimen SEN 1

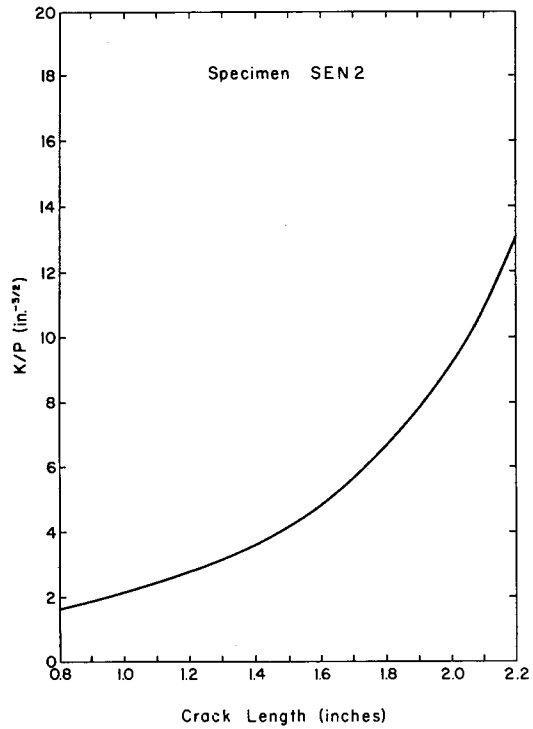


Fig. 3 - Stress intensity relationship between applied load and crack length for specimen SEN 2

Load Control and Crack Measurement

A closed-loop, hydraulically actuated, servo-controlled mechanical test system with a 20-kip load cell and 50-kip load frame was used to apply the loads within 1 percent of the desired values. By decreasing the loads stepwise according to Figs. 2 or 3, constant average stress intensity values were applied to the specimen for a given crack length change. Crack lengths were visually measured on the specimen's surface using a 10X traveling microscope calibrated to read 0.0001-in. increments. Because the corrosion products clouded the electrolyte solution or adhered to the specimen surface during the test, it was difficult to maintain this accuracy in crack length measurements. The data have been reported as the average of several observations, so that some of the random error in measuring crack lengths has been eliminated. The average crack growth rates reported herein are felt to be at least within 10 percent of their population mean.

Environments

The base line fatigue crack propagation rates were obtained in a vacuum chamber that completely surrounded the specimen. A liquid nitrogen cold trap used in conjunction with a high vacuum diffusion pump provided a vacuum of 1×10^{-7} torr in less than 4 hours. The system was allowed to pump down for about 8 hours prior to data collection; consequently, the data were collected in a vacuum somewhat less than 1×10^{-7} torr.

The freely corroding crack propagation data were obtained using a 3.5% sodium chloride solution that was prepared from reagent grade sodium chloride and distilled water. The pH of the freshly made solution varied between 6.5 and 6.8. The environmental chamber used to contain the corrosive solution was an open acrylic plastic box (3 by 4.5 by 1.5 in.). The specimen was inserted into a centrally located hole in the bottom of the box and was positioned so the crack plane was approximately 1/2 in. above the bottom; the chamber was sealed into position using pyseal wax. The corrosive solution was open to the atmosphere and was maintained at ambient temperature.

The coupling sacrificial anodes used in the HY-80 investigation were of cadmium, zinc, and magnesium. Two anodic electrodes were placed on the floor of the environmental box, one on each side of the specimen. Electrochemical potentials were continuously monitored using a silver-silver chloride reference electrode coupled to a strip chart recorder having a 10^6 - Ω input impedance. The ranges of measured potential and most frequently measured values are given in Table 2.

Table 2
Electrochemical Measurements in HY-80 Study

Environmental Condition	Lowest Reading (V)	Usual Reading (V)	Highest Reading (V)	Change in Potential During Test
Freely corroding	-0.59	-0.64	-0.665	More negative
Cadmium anode	-0.715	-0.735	-0.775	More positive
Zinc anode	-1.035	-1.04	-1.05	Constant
Magnesium anode	-1.25	-1.36	-1.38	More positive

To study the influence of buffered solutions on the above- $K_{I_{sc}}$ corrosion fatigue behavior, a 0.025M borax buffer with 3.5% sodium chloride added was prepared according to the schedule given below (7). The resulting pH of this solution was 8.3.

1. Add 9.5343 g of sodium tetraborate decahydrate (formula $\text{Na}_2\text{B}_4\text{O}_7 \cdot 10\text{H}_2\text{O}$) to 1 liter of distilled water (0.025M borax solution).
2. Dilute 8.6 ml concentrated hydrochloride acid with distilled water to prepare 1 liter 0.1M HCl solution.
3. Mix 100 ml of 0.025M borax solution with 30 ml of 0.1 HCl solution to obtain 8.5 pH buffer.
4. Add 35 g sodium chloride per liter of the borax buffer.

RESULTS AND DISCUSSION

The results of a series of fatigue crack propagation tests are summarized and discussed in this section. For purposes of discussion, it is somewhat easier to present the data in the following order: fatigue in vacuum behavior, corrosion fatigue behavior below $K_{I_{scc}}$, and corrosion fatigue behavior above $K_{I_{scc}}$. These separate categories can be used in general to isolate the cycle-dependent fatigue-controlled behavior, an environment-fatigue interaction behavior, and a time-dependent, environmentally controlled behavior. The purpose of the report is to investigate the influence of combined environment and fatigue effects and to compare the behaviors observed in the separate categories. The base line fatigue behavior in vacuum is presented first.

Fatigue in Vacuum

The base line fatigue-crack propagation rates obtained in a hard vacuum (1×10^{-7} torr) are presented in Fig. 4. The 4340 steel data were collected at a frequency of 10 Hz using a zero-tension square-wave cycle. The HY-80 trend line indicated in the figure

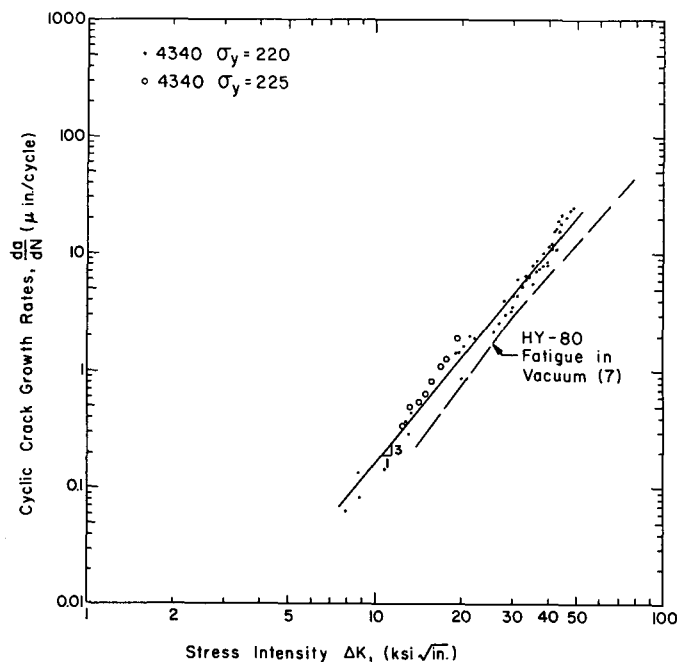


Fig. 4 - Fatigue crack growth rates collected in a 1×10^{-7} torr vacuum for HY-80 and 4340 steel

was obtained from data collected at 18 Hz for sinusoidal loading by Meyn (8) using the same vacuum system described above. Included in Fig. 4 are additional 4340 data (8) collected for a slightly higher yield strength (225 ksi). The only noticeable difference between the rates of the three materials is that the higher yield strength 4340 steel has a slightly faster crack growth rate.

The vacuum rates are substantially slower than the reported rates for the two materials in laboratory air (9,10). Since air contains water vapor and oxygen, it represents a potentially aggressive environment; water and oxygen could react with the newly forming fatigue crack surfaces to give an enhanced crack growth. Because the exact environmental dependence of air fatigue crack growth is not known, air data should not be used as a quantitative base line for corrosion fatigue studies.

Corrosion Fatigue Crack Growth Rates Below K_{Isc}

Effect of Frequency — The mistake that an investigator can make in evaluating corrosion fatigue resistance by testing at one loading frequency (especially at a high one) can be conveyed by the zero-tension data shown in Fig. 5, where all the rates were obtained at a frequency of 10 Hz. These HY-80 data were collected in a 3.5% NaCl solution using haversine load waveforms with a 200 lb minimum load.

Included for reference in Fig. 5 are the upper and lower limits of the Barsom *et al.* scatter band (10). This band had been shown to bracket the large quantity of published steel fatigue crack propagation data (including that of HY-80) obtained in air. Notice that the corrosion fatigue data presented in Fig. 5 lie close to the vacuum trend line and are

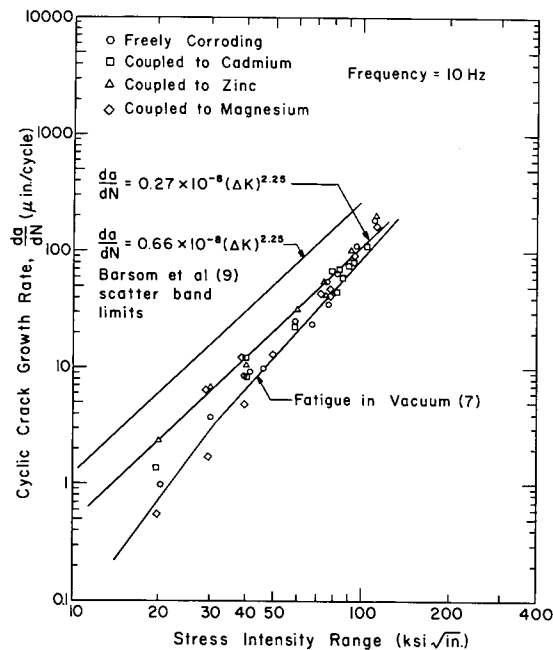


Fig. 5 - The corrosion fatigue crack growth rates in HY-80 collected at a frequency of 10 Hz are compared to vacuum rates (8) and the Barsom *et al.* (10) fatigue in air scatter band

below or at the bottom of the fatigue in air scatter band. An investigator might conclude from the figure that HY-80 steel has good corrosion fatigue resistance and that cathodic protection has a minor effect on the rate of crack growth.

The fallacy of such conclusions is shown by the data presented in Fig. 6, where the cyclic crack growth rate is shown to increase with decreasing frequency to a rate five to six times faster than the base line rates for two different values of stress intensity range. To establish the cyclic crack growth rate behavior for the frequency range investigated (0.001 to 10 Hz), two levels of stress intensity range ($\Delta K = 39$ and $78 \text{ ksi } \sqrt{\text{in.}}$) were thought sufficient. Such a choice resulted in cost saving for both the number of specimens used and the time spent in data collection. The previous statement could only be made if the growth behavior pattern did not change significantly between the two levels.

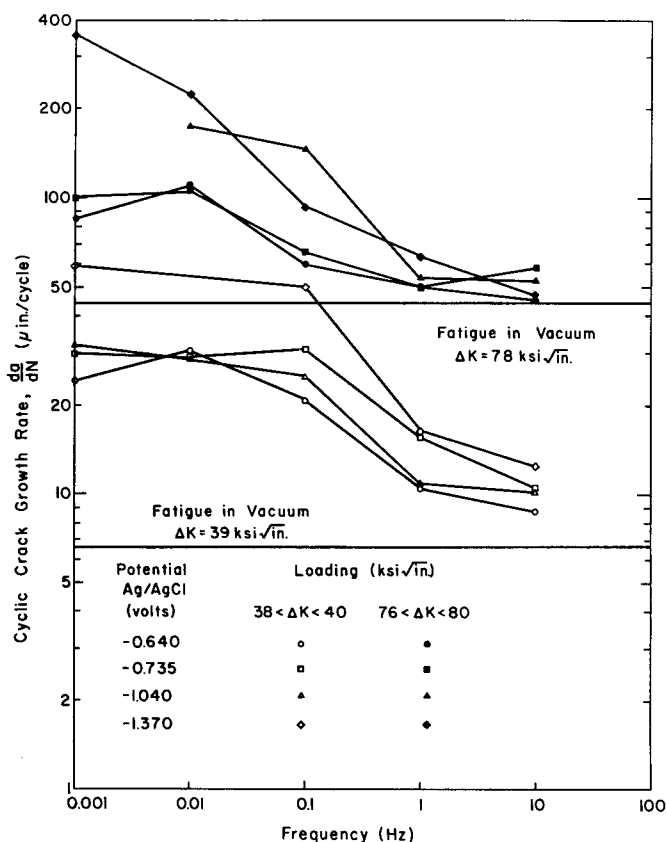


Fig. 6 - Corrosion fatigue cyclic crack growth rates in HY-80 as a function of frequency

The corrosion fatigue crack growth rates for the HY-80 steel presented in Figs. 5 and 6, as well as those introduced later, represent the average of several values, except at the 0.001-Hz frequency where only one value was collected because of the length of test (220 cycles).

The variation of corrosion fatigue behavior shown in Figs. 5 and 6 should not be considered new. In 1932, Gough (11) noted from observations based on McAdam's data that the relative corrosion fatigue resistances offered by the same metal exposed to two

different environments of varying corrosivity may be completely altered by a change in cyclic frequency, the reason again being that two coexisting phenomena are acting, one cycle dependent, the other time dependent.

To determine the trends in behavior, compare any two of the curves in Fig. 6 showing the constant-environment corrosion fatigue rate vs frequency. A comparison shows that the corrosion fatigue growth rates at the high ΔK are greater than the corresponding rates at the low ΔK as expected. In general, however, the ratio of corrosion fatigue rate to vacuum rate indicates that the maximum environmental growth enhancement occurs at the lower stress-intensity ranges. The data indicate that the corrosion fatigue cyclic crack growth rates merge to the vacuum rates at high levels of ΔK .

Crooker and Lange (12,13) have recently published comparative studies of salt water corrosion fatigue and air fatigue cracking behaviors for six 180-ksi yield-strength steels having moderately high $K_{I_{sc}}$ values. The data were collected for a wide variation in stress-intensity range at a constant frequency of 5 cycles/min (0.083 Hz). Five of the six steels investigated showed a merging of the salt water corrosion fatigue crack growth rate data to the air data at higher levels of ΔK (the maximum cyclic stress intensity was still lower than $K_{I_{sc}}$). The corrosion fatigue crack growth data for the other steel (9Ni-4Co-0.25C) indicated immunity to the salt water environment when compared to air fatigue data.

Barsom (14) has reported on the effect of salt water corrosion fatigue crack propagation below $K_{I_{sc}}$ in a 12Ni-5Cr-3Mo steel (yield stress, 184 ksi; $K_{I_{sc}}$, 60 ksi $\sqrt{\text{in.}}$). His data were collected for a variation of ΔK between 15 and 50 ksi $\sqrt{\text{in.}}$ for three frequency levels (0.1, 1, and 10 Hz). The results of his study indicate that the ratio of corrosion fatigue to air fatigue cracking rate was constant for a constant environmental condition and for a constant frequency; he proposes that this behavior represents a hypothesis for below- $K_{I_{sc}}$ behavior. The results presented here as well as those by Crooker and Lange (12,13) do not substantiate this hypothesis. Possibly the constant-ratio trend in crack growth rate behavior only exists for certain ranges of ΔK or for specific material-environment systems.

As indicated by Fig. 6, the rate of cyclic crack growth in most of the environments tested appears to reach an upper limit at a frequency of 0.01 Hz for the cracking rates collected at the high ΔK and of 0.1 Hz for the low ΔK data. If, as suggested by the data in Fig. 6, there is a characteristic frequency at which the cyclic crack growth rates reach a maximum, the nature of the time-dependent component of the corrosion fatigue attack mechanism would also change at this frequency.

As the frequency is lowered, the nature of the environmental attack will change if

1. A crack surface film developed which either inhibited the cathodic reaction or changed the chemistry of the local corrosion cell at the crack tip.
2. The electrochemistry of the local cell at the crack tip promoted blunting or uniform attack of the crack surface.
3. A slow step in a hydrogen diffusion and reaction sequence limited the volume of hydrogen-embrittled material at the crack tip.

Additional low-frequency experiments are required to discern which of these hypotheses provides the best description of the environmental cracking mechanism.

Time-Based Cyclic Crack Growth Rates Below $K_{I_{sc}}$ — Multiplying the cyclic crack growth rates given in Fig. 6 by the corresponding loading frequency results in the

time-based crack-extension behavior illustrated in Fig. 7. The behavior described in Fig. 7 indicates that the time required to extend a crack a fixed distance increases approximately one order of magnitude for every one order of magnitude decrease in loading frequency. This type of behavior may be characteristic of below- K_{Isc} behavior; i.e., predominately cycle-dependent fatigue crack growth behavior. The cycle-dependent behavior implies that the localized environmental attack will only take place when the crack is extended by the fatigue mechanism.

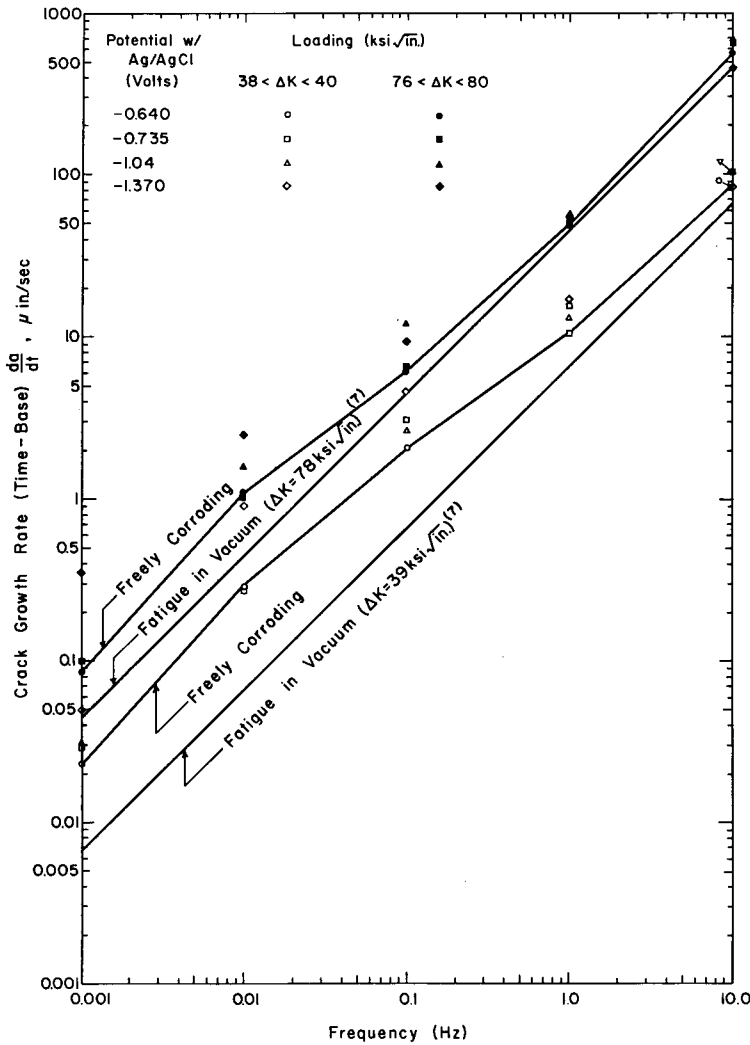


Fig. 7 - Time-based corrosion fatigue crack growth rates in HY-80 as a function of frequency—below- K_{Isc} behavior

For many structures that experience slow loading frequencies over long periods of time, the type of corrosion fatigue damage illustrated in Fig. 7 would be significant from an engineering standpoint. For such cases, the design approach outlined by Sinclair and Rolfe (15) could be used to establish inspection periods and to predict component life. To estimate the corrosion fatigue rates for the low-strength, high-toughness materials

loaded at low frequencies to stress intensity levels below $K_{I_{sc}}$, one could use the data presented in Figs. 6 and 7 and that collected by Barsom (14) and by Crooker and Lange (12,13). A useful rule of thumb might be that the corrosion fatigue crack growth rates for stress-intensity levels below $K_{I_{sc}}$ are less than ten times faster than the fatigue crack propagation rates in air.

Effect of Electrochemical Potential — As early as 1943, Evans (16) conceived that corrosion fatigue resistance could be reduced in environments where the cathodic reaction is evolution of hydrogen. The question which Evans posed was: Could hydrogen embrittlement damage be introduced by the standard methods of sacrificial protection? Early corrosion fatigue studies on smooth specimens showed that materials retain most if not all of their (air value) fatigue life when cathodic protection is applied to the specimen (17). Smooth specimen fatigue behaviors typically represent the overall effect of a process on the nucleation and propagation of cracks; there is no separation of the effects that the process has on each prefailure stage. Monitoring crack length changes in pre-cracked specimens while controlling the logical mechanical parameter, the stress intensity, provides a quantitative method of interpreting the effect of cathodic protection on corrosion-fatigue crack-growth rates. Furthermore, a study of crack propagation coupled with smooth specimen behavior can be used to provide a qualitative understanding of the crack initiation process.

The data given in Fig. 6 have been replotted in Figs. 8 and 9 to show the effect of varying the electrochemical potential at each frequency of loading. The trend of the data indicates that the cyclic crack growth rate increases as the electrochemical potential becomes more electronegative. In sustained-load stress-corrosion cracking studies, when such crack extension behavior is observed, the mechanism of attack has been suggested to be hydrogen embrittlement (18,19). The logic behind the theory is that decreases in electrochemical potential promote decreasing dissolution rates and increasing supplies of hydrogen (18).

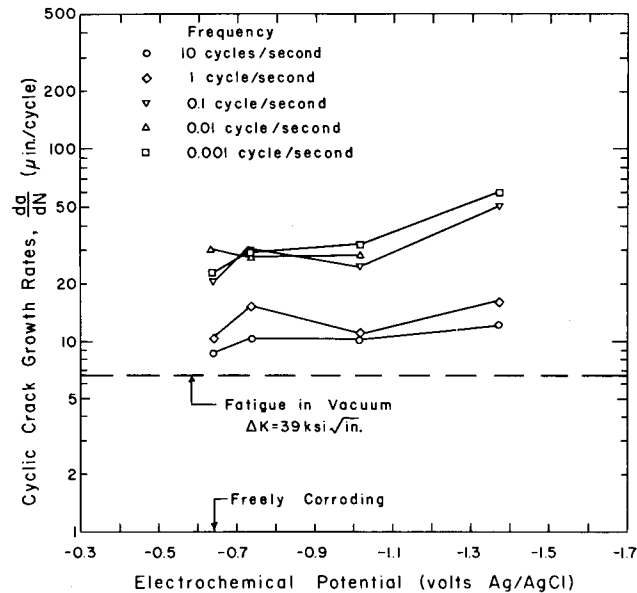


Fig. 8 - Corrosion fatigue crack growth rates in HY-80 as a function of electrochemical potential for the low amplitude fatigue loading ($\Delta K \approx 39 \text{ ksi } \sqrt{\text{in.}}$)

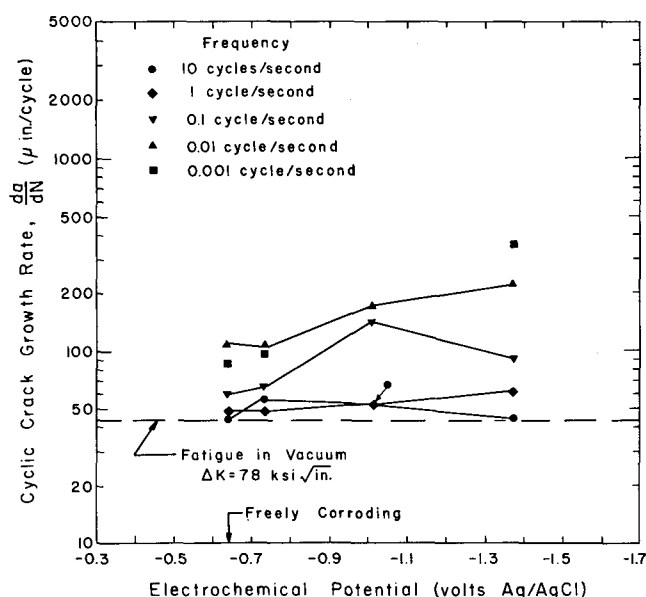


Fig. 9 - Corrosion fatigue crack growth rates in HY-80 as a function of electrochemical potential for the high amplitude fatigue loading ($\Delta K \cong 78 \text{ ksi } \sqrt{\text{in.}}$)

Because the corrosion-fatigue growth rates are significantly larger than the vacuum rates at the lower frequencies, the effects of cathodic protection are more noticeable here. A comparison of the constant-frequency curves in Figs. 8 or 9 indicates that the ratios between the various constant-environment crack growth rates do not change substantially with frequency changes below 1 Hz. Listed in Table 3 are cyclic growth rate ratios between the freely corroding and magnesium anode conditions at various frequencies. With decreasing frequency, these crack growth rate ratios are seen to increase, but only slightly. This is surprising because hydrogen embrittlement phenomena are characteristically strain rate sensitive (20). Possibly, the main influence of hydrogen is already suitably reflected in the freely corroding crack growth rate behavior. In summary, applying cathodic protection to HY-80 steel with sacrificial anodes results in an increase of the rate of cyclic crack growth above the freely corroding rate.

The schematic diagram of the time to fail vs the electrochemical potential shown in Fig. 10 represents the smooth specimen fatigue behavior of HY-80 steel (21). These specimens were reverse-bend tested at a frequency of 1 cycle/min in a 3.5% NaCl solution while subjected to cathodic protection potentials. As indicated in Fig. 10, a potential slightly more electronegative than the freely corroding potential yields a maximum specimen life under constant stress conditions.

The type of smooth-specimen fatigue behavior shown in Fig. 10 differs substantially from that observed in the early studies of structural steel behavior, where applied cathodic potentials were shown to result in the recovery of the air fatigue life (17). These structural steel corrosion fatigue data were for the most part generated at high frequencies (between 30 and 100 Hz). If the results of these earlier studies are reinterpreted in light of the low-frequency HY-80 smooth specimen and crack growth rate behaviors, one must conclude that the protection offered by applying cathodic potentials to a material undergoing corrosion fatigue action is one of delaying the nucleation of surface cracks.

Table 3
Ratio of Changes in Crack Growth Rates
HY-80 Steel Fatigue

ΔK (ksi $\sqrt{\text{in.}}$)	Frequency (Hz)	Cracking Rate Ratio*
40	0.001	2.08
40	0.01	3.2
40	0.1	2.24
40	1.0	1.58
80	0.001	3.92
80	0.01	2.28
80	0.1	2.0
80	1.0	1.12

*Ratio of Mg-coupled crack growth rate to freely corroding crack growth rate.

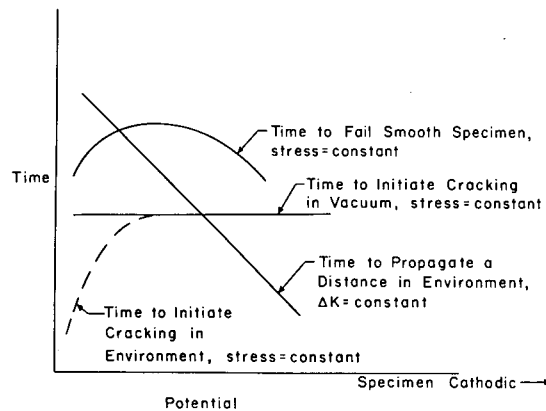


Fig. 10 - Schematic diagram of the influence of electrochemical potential on initiation and propagation of cracks to failure of smooth specimens

Since the cathodic potentials were developed by sacrificial action for both the smooth specimen and crack growth HY-80 investigations, a hypothesis based on inhibiting the crack nucleation process is reasonable. Most of the protection given to steel by sacrificial anodes of cadmium, zinc, aluminum, and magnesium is by physical exclusion of the corrodent (22). Inorganic cations can precipitate out as hydroxides or carbonates at the basic cathode and form a tight layer which acts as a diffusion barrier to oxygen and leads to high cathodic polarization (22). Since the results of the crack propagation study indicate that the cracking rate increased as the electrochemical potential became more negative, it is reasonable to suggest that the local cell conditions in crevices and cracks might prevent complete surface coverage by the cation barrier and provide sites for hydrogen to become absorbed and cause embrittlement.

Figure 10 presents a summary of what is known or suspected about the smooth specimen corrosion fatigue behavior of structural steels. The time to nucleate a crack and the time to grow a crack a fixed distance under controlled mechanical conditions in an aqueous environment increases and decreases, respectively as the electrochemical potential decreases. The time to fail a smooth specimen will represent the composite influence of the environment on the initiation and propagation of cracks.

Corrosion Fatigue Crack Growth Rates Above K_{Isc}

The purpose of this phase of the investigation was to provide crack propagation information which could be compared or contrasted to the data generated in the HY-80 phase. As suspected, the corrosion fatigue crack propagation behavior of 4340 steel provides more contrast than comparison to the HY-80 behavior. While the 4340 material exhibits a sustained-load crack growth pattern with a K_{Isc} of approximately $10 \text{ ksi } \sqrt{\text{in.}}$ (see Fig. 11), valid measurements of the K_{Isc} for HY-80 have not yet been obtained (a value greater than $200 \text{ ksi } \sqrt{\text{in.}}$ would be a rough estimate). One would correctly guess that the environmental effect on the corrosion fatigue crack growth behavior depends on the level of stress intensity with respect to K_{Isc} . All stress intensity levels in the HY-80 investigation were well below the estimated K_{Isc} of that material.

In the 4340 investigation, square wave loading cycles were applied to the SEN 2 specimens to produce corrosion fatigue crack growth rates under constant maximum stress intensity conditions. The applied "zero" to tension load cycle had a 0.015-sec rise time and a 200-lb minimum load. Two stress intensity levels ($K_{max} = 20$ and $40 \text{ ksi } \sqrt{\text{in.}}$) were chosen to illustrate the crack propagation behavior. The frequency was varied through several orders of magnitude to establish environmental dependence.

The sustained-load crack extension behavior shown in Fig. 11 was determined for the lowest frequency studied, i.e., at 0.005 Hz. Crack growth rates were calculated by dividing the change in crack length by the time that the static load was applied. Crack extension for each applied stress intensity level was usually greater than 0.02 in., except for those data collected at applied stress intensity levels below $11.5 \text{ ksi } \sqrt{\text{in.}}$ where the crack extension was 0.005 in.

In Fig. 11, it appears that there are three regions where the stress-corrosion cracking rate has a specific pattern. In the two regions where the static stress intensity level is below $13 \text{ ksi } \sqrt{\text{in.}}$ or above $42 \text{ ksi } \sqrt{\text{in.}}$, the crack growth rate changes drastically for small changes in the stress intensity level. The stable crack growth region between the stress intensity limits of 13 and $42 \text{ ksi } \sqrt{\text{in.}}$ could be termed the plateau region.

Because cracking rates are more reproducible in the plateau region than in the outer regions, environmental variables are easier to study in this region. For example,

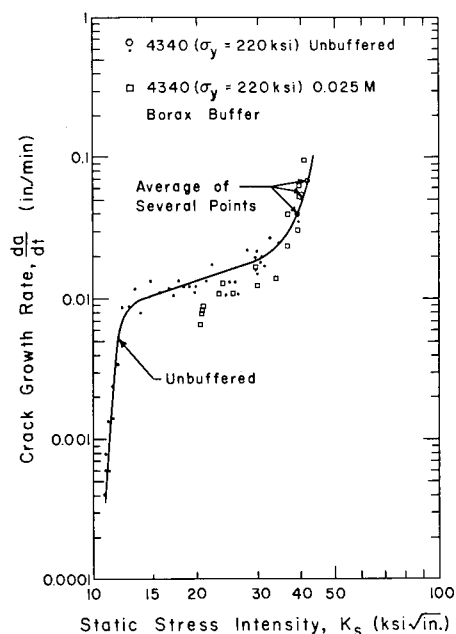


Fig. 11 - Sustained-load crack growth rates in 4340 steel for two 3.5% NaCl solutions (unbuffered and buffered with borax)

changing the environment to a 0.025M borax buffer with 3.5% NaCl, the sustained load crack growth rate pattern assumed the form indicated in Fig. 11. Comparing the crack growth rate patterns exhibited by the 4340 material indicates that the main effect of changing environments was to shift the level of K_{Isc} from 10 to 20 ksi $\sqrt{\text{in.}}$. It is also seen in Fig. 11 that the cracking rates in the plateau region for the buffered environment are slightly lower than the corresponding rates in the unbuffered 3.5% NaCl solution.

The corrosion fatigue crack growth rates obtained by square wave loading ($\Delta K \approx K_{max} = 20$ and 40 ksi $\sqrt{\text{in.}}$) the 4340 specimens at several frequencies are shown in Fig. 12. The crack growth rates presented in this figure represent an average of at least five values and were obtained by multiplying the crack length change by the ratio of frequency to the number of applied load cycles.

The cyclic crack growth rates given in Fig. 12 are seen to be independent of the number of applied load cycles; i.e., they are cycle independent, and the behavior therefore simulates sustained crack growth rate behavior. Note that the sustained load crack growth rate conversion factor between Figs. 11 and 12 is 1/2. Included in Fig. 12 for reference are two lines which represent the cycle-dependent vacuum fatigue behavior for stress intensity ranges of 20 and 40 ksi $\sqrt{\text{in.}}$. These lines were extrapolated from the vacuum data presented in Fig. 4.

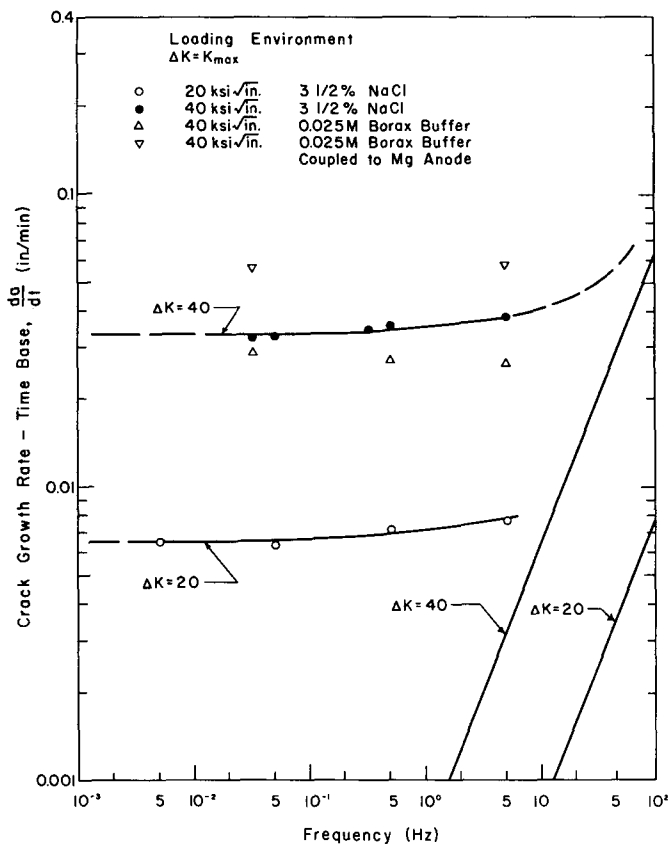


Fig. 12 - Time-based crack growth rates in 4340 steel as a function of frequency—above- K_{Isc} behavior

Because the sustained crack growth rates were much faster than the vacuum cyclic crack growth rates at the frequencies studied, it was not possible to exhibit the complete fatigue crack growth rate behavior using square wave loading. The dashed curves indicate the expected behavior for frequencies higher than those studied. At the higher frequencies, the environmental fatigue crack growth rates are expected to merge with the vacuum fatigue crack growth rates. Notice the contrast in time-based corrosion fatigue crack propagation behaviors exhibited by the two steels as made clear by the data presented in Figs. 7 and 12. The HY-80 steel was previously noted to crack in a cycle-dependent manner for all the frequencies studied when the stress intensity range was below K_{Isc} . As illustrated by Fig. 12, the 4340-steel corrosion fatigue data indicate that a cycle-independent cracking takes place for stress intensity levels above K_{Isc} (restricted to frequencies below 1 Hz). These two figures (Figs. 7 and 12) provide a summary description of the characteristic behaviors of the above- and below- K_{Isc} regimes of corrosion fatigue crack propagation.

The results of this above- K_{Isc} study and those by Gallagher and Sinclair (23) and Wei and Landes (24) indicate that the Wei and Landes hypothesis provides a reasonable estimate of the above- K_{Isc} corrosion fatigue behavior of steels. This hypothesis suggests that environmentally-induced fatigue crack propagation rates can be directly obtained by adding the sustained-load influence of the aggressive environment to the fatigue crack growth rate obtained in an inert environment on a cyclic basis. This hypothesis only applies to above- K_{Isc} cracking behaviors, because by definition there is no sustained-load crack growth below K_{Isc} (3).

The usefulness of the Wei and Landes hypothesis should be immediately evident for design purposes. Interaction should only be expected between the sustained-load and fatigue cracking mechanisms when the sustained-load cracking rate is within an order of magnitude of the corresponding inert-environment fatigue crack growth rate. Having data which are similar to those presented in Figs. 4 and 11 for a material-environment system, a designer will be able to determine the frequency at which the environment starts to influence the cycle-dependent fatigue crack growth rate. If this frequency is well below the frequency of loading experienced by the structure, then a design analysis based on fatigue behavior alone would be adequate.

As can be noted from Fig. 12, changes in environmental conditions influence the magnitude of cracking but not the behavioral pattern. The borax buffer environment reduced the magnitude of corrosion fatigue crack growth rates by the same amount that it had reduced the sustained-load cracking rates in the plateau region of Fig. 11. Coupling the 4340 steel specimen to a sacrificial magnesium anode accelerated the corrosion fatigue crack growth rate in the borax buffer by a factor of about 2. This result was striking because the corrosion fatigue crack growth rates of HY-80 were also increased by approximately the same factor when the material was coupled to a magnesium anode (see Table 3). It is possible that this result should not have been unexpected, if hydrogen embrittlement is responsible for the enhanced crack growth rates in both steels.

CONCLUSIONS

Subjected to the limitations imposed within this report, the following conclusions appear reasonable:

1. Corrosion fatigue crack propagation of HY-80 steel in 3.5% NaCl is influenced by the electrochemical potential; in general, the more electronegative the potential, the higher the rate of crack propagation.

2. In HY-80 steel, the rate of environmental attack increases (as evidenced by the change in cyclic crack propagation rates) with decrease in loading frequency from 10 to 0.01 Hz. The rate of environmental attack for a loading frequency of 0.001 Hz was approximately equal to the rate at 0.01 Hz, indicating a possible leveling off or decrease in environmental attack.

3. The corrosion fatigue crack propagation behavior of the 4340 steel is markedly different from that of the HY-80 steel, mainly because in the 4340 investigation the stress intensity levels were above $K_{I_{sc}}$, where the environmental attack controls the rate of crack growth.

4. Fatigue crack propagation rates in vacuum for the two materials do not differ greatly. The lower strength material exhibited a slightly lower crack propagation rate than the higher strength 4340.

5. Changes in load frequency will change crack propagation rates from a time-dependent to a cycle-dependent process in materials loaded to stress intensity levels above $K_{I_{sc}}$. The changeover frequency occurs when the low-frequency corrosion fatigue crack propagation rate is within an order of magnitude of the time-based fatigue crack propagation rate (rates measured at corresponding stress intensity levels).

6. Buffering the 3.5% NaCl solution with a 0.025M borax buffer to a pH of 8.3 doubled the measured $K_{I_{sc}}$ from 10 to 20 ksi $\sqrt{\text{in.}}$ and slightly reduced the sustained-load crack propagation rates in the plateau region. There was no change in the corrosion fatigue crack growth rate behavior in the plateau region.

7. The crack propagation rates measured for the magnesium-coupled condition was approximately twice the freely corroding rates (at any given frequency and ΔK level) for both steels.

ACKNOWLEDGMENT

The author expresses his sincere thanks to the team of coworkers in the Physical Metallurgy Branch of Metallurgy Division of NRL who made this investigation possible. The encouragement and stimulation offered by B. F. Brown and D. A. Meyn were beyond a summer employee's fondest hopes.

REFERENCES

1. Gilbert, P.T., "Corrosion-Fatigue," *Metallurgical Rev.*, 1(No. 3):379 (1956)
2. Johnson, H.H., and Paris, P.C., "Sub-Critical Flaw Growth," *J. Engrg. Fracture Mech.*, 1(No. 1):3 (1968)
3. Brown, B.F., "A New Stress-Corrosion Cracking Test for High-Strength Alloys," *Materials Res. Standards*, 6(No. 3):129 (1966)
4. Dahlberg, E.P., "Fatigue-Crack Propagation in High-Strength 4340 Steel in Humid Air," *Trans. ASM*, 58:46 (1965)
5. Mulherin, J.H., "Stress-Corrosion Susceptibility of High-Strength Steel in Relation to Fracture Toughness," *J. Basic Engrg.*, *Trans. ASME*, 88(Series D):777 (1966)
6. Gallagher, J.P., "Experimentally Determined Stress Intensity Factors for Several Contoured Double Cantilever Beams," *J. Engrg. Fracture Mech.*, 2 (in preparation)
7. Weast, R.C., editor, "Handbook of Chemistry and Physics," 47th ed., 1966, p. D-79
8. Meyn, D.A., unpublished results, 1968
9. Miller, G.A., "The Dependence of Fatigue-Crack Growth Rate on the Stress Intensity Factor and the Mechanical Properties of Some High-Strength Steels," *Trans. ASM*, 61:442 (1968)
10. Barsom, J.M., Imhof, E.J., Jr., and Rolfe, S.T., "Fatigue Crack Propagation in High-Strength Steels," submitted for publication to *J. Engrg. Fracture Mech.*, 1969
11. Gough, H.J., "Corrosion Fatigue of Metals," *J. Inst. Metals*, 49:17 (1932)
12. Crooker, T.W., and Lange, E.A., "Corrosion Fatigue Crack Propagation Studies of Some New High-Strength Structural Steels," *NRL Report 6870*, April 1969
13. Crooker, T.W., and Lange, E.A., "Fatigue Crack Growth in Three 180-ksi Yield Strength Steels in Air and in Salt-Water Environments," *NRL Report 6761*, Sept. 1968
14. Barsom, J.M., "Investigation of Subcritical Crack Propagation," Unpublished Doctoral Dissertation, College of Engineering, University of Pittsburgh, June 1969
15. Sinclair, G.M., and Rolfe, S.T., "Analytical Procedure for Relating Subcritical Crack Growth to Inspection Requirements," Technical Report, Applied Research Lab., United States Steel, Project No. 39.018-007(26), Jan. 2, 1969, AD 846116L
16. Stuart, N., and Evans, U.R., "The Effect of Zinc on the Corrosion-Fatigue Life of Steel," *J. Iron Steel Ind.* 147:131 (1943)
17. Evans, U.R., and Simnad, M.T., "The Mechanism of Corrosion Fatigue of Mild Steel," *Proc. Roy. Soc.*, A(188):372 (1947)

18. Brown, B.F., "Implication of Cathodic Reduction of Hydrogen to Stress-Corrosion Cracking," abstract of topic presented to The Electrochemical Society Meeting, Detroit, Oct. 1969
19. "A Review of the Stress-Corrosion Behavior of Steels with High Yield Strength," from Proc. Conf. on Fundamental Aspects of Stress-Corrosion Cracking, edited by Staehle, Forty, and Van Rooyen, NACE, Houston, 1969, pp. 398-410
20. Cotterill, P., "The Hydrogen Embrittlement of Metals," from "Progress in Metal Physics," B. Chalmers, editor, New York:Pergamon, 1961, Vol. 19, p. 201
21. Smith, J.A., Peterson, M.H., and Brown, B.F., "Effect of Cathodic Protection on Low-Cycle Corrosion Fatigue of HY-80 Steel at Slow Cycle Rates," NRL Memo Report 1302, April 1962
22. Cole, H.G., "Effect of Mechanical Factors on Corrosion," from "Corrosion," L.L. Shreir, editor, New York:Wiley, 1963, p. 8.52
23. Gallagher, J.P., and Sinclair, G.M., "Environmentally Assisted Fatigue Crack Growth Rates in SAE 4340 Steel," ASME Paper No. 69-MET-9 (to appear in J. Basic Engrg., Trans. ASME 91 (Series D, No. 4):598 (1969)
24. Wei, R.P., and Landes, J.D., "Correlation Between Sustained-Load and Fatigue Crack Growth in High-Strength Steels," Materials Res. Standards, 9(No. 7):25 (1969)